Int. J. Electron. Commun. (AEÜ) 112 (2019) 152942

Contents lists available at ScienceDirect

International Journal of Electronics and Communications (AEÜ)

journal homepage: www.elsevier.com/locate/aeue

Regular paper

Band-pass filters based on periodic structures in SIW technology

J. Martínez [a], Á. Coves [a], E. Bronchalo [a], Á.A. San Blas [a,*], M. Bozzi [b]

[a] Dpto. de Ingeniería de Comunicaciones-I3E, Universidad Miguel Hernández de Elche, 03202 Elche, Alicante, Spain
[b] Department of Electrical, Computer and Biomedical Engineering, University of Pavia, Italy

ARTICLE INFO

Article history:
Received 27 June 2019
Accepted 2 October 2019

ABSTRACT

In this work, the study of two different topologies of S-band band-pass filters based on periodic structures in substrate integrated waveguide (SIW) technology is theoretical and experimentally addressed. The first topology consists of periodic rectangular perforations of the SIW substrate. In this filter topology, the lower cutoff frequency is determined by the cutoff frequency of the first Floquet mode of the periodic structure, while the upper cutoff frequency and the rejection band are conditioned by its first band-gap. The second topology consists of a periodic array of square complementary split-ring resonators (CSRRs) etched on the waveguide surface. In this case, the use of subwavelength resonators with evanescent-wave transmission leads to a much smaller filter, given that the pass-band is below the cutoff frequency of the waveguide. The effect of the different dimensions of the unit cell in the filters characteristics (lower cutoff frequency, pass-band, and rejection-band associated to the first band-gap of the periodic structure) is analyzed through the dispersion diagram of the periodic cell. Finally, two band-pass filters based on each topology have been designed and built, showing in both cases good matching and low insertion loss in the pass-band, and a deep rejection band.

1. Introduction

Periodic structures in waveguiding systems (also called Electromagnetic Band Gap (EBG) structures) show very attractive filtering properties in the frequency domain associated with the appearance of permitted and forbidden frequency bands in their dispersion diagram, yielding size reduction and rejection band improvement. There are many examples of periodic structures with filtering applications [1–6].

In the last two decades, many works have been published on the Substrate Integrated Waveguide (SIW) technology [7,8]. In the field of filter design, SIW structures have been adopted in a great variety of filter topologies [9–11]. Several SIW-EBG filters using various techniques have been presented in last years [12–14]. Recently, a new filter topology based on perforations of the dielectric substrate has been developed [15–17], adding flexibility to the designs and extending this concept to half-mode and folded structures.

In this work, EBG structures in SIW technology are applied to the analysis and design of two band-pass filters in S-band with different types of periodic cell, in order to highlight their advantages and disadvantages. The first filter is based on the realization of periodic rectangular perforations of the dielectric substrate of the SIW, a technique first proposed for C-band [18]. In the second SIW filter, square complementary split-ring resonators (CSRRs) [19–22] are periodically etched on the waveguide surface.

In Section 2, we present the analysis of the dispersion diagram of the unit cell for both periodic structures, showing the dependence of the first pass-band and stop-band on the different unit cell parameters. In Section 3, two periodic filters are presented based on each unit cell topology, highlighting their differences in terms of size and electrical response. Finally, the conclusions of the work are summarized in Section 4.

2. Dispersion characteristics of the periodic SIWs under study

In order to characterize a periodic structure in the frequency domain, the dispersion diagram associated to its unit cell must be calculated [1,23]. This has been done for the two periodic structures presented in this work by using the commercial software tool Ansys HFSS (see, for instance, [15,24]). The two SIW structures have in common the substrate and the vias dimensions. The substrate is Taconic RF-10 (relative permittivity $\epsilon_r = 10, \tan\delta = 0.0035$) with a height $b = 0.63$ mm. The vias defining the lateral walls of the SIW have diameter $d_s = 0.8$ mm and separation $s_v = 1.2$ mm, which guarantees negligible radiation losses.

* Corresponding author.
E-mail addresses: javier.martinez35@alu.umh.es (J. Martínez), angela.coves@umh.es (Á. Coves), ebronchalo@umh.es (E. Bronchalo), aasanblas@umh.es (Á.A. San Blas), maurizio.bozzi@unipv.it (M. Bozzi).

https://doi.org/10.1016/j.aeue.2019.152942
1434-8411/

2.1. SIW with periodic rectangular perforations of the substrate

The first configuration of periodic SIW studied, whose unit cell is shown in Fig. 1, has been built by periodically perforating the substrate with rectangular profile perforations. The waveguide of period D has width a_{siw}, being the perforated rectangle of dimensions $D/2 \times w$. We have chosen a waveguide width $a_{siw} = 23$ mm, and the same value for the period $D = 23$ mm for simplicity. For this width, the cutoff frequency is 2 GHz for the initial SIW (without perforations), and it increases with the volume ratio air/substrate of the unit cell, as it will be seen next. For this case, we have studied the influence of the rectangular air holes width w on the dispersion diagram, thus providing different effective permittivity values in the perforated sections. As it is well-known, the modification of the effective permittivity contrast within the periodic cell has a direct effect on the dispersion behaviour of the periodic waveguide [25], both in terms of the cutoff frequency and the band-gap width and position. Fig. 2 shows the dispersion diagram of a periodically perforated SIW with $a_{siw} = D = 23$ mm for different rectangle widths. As it can be appreciated, the cutoff frequency of the waveguide increases with w. This is due to the fact that the average permittivity in the periodic cell diminishes with w. On the other hand, it can also be observed in Fig. 2 that the first band-gap of this waveguide widens significantly with the parameter w. This behavior has already been explained in [23], where it is shown that the band-gap width of the periodic structure is higher for higher permittivity contrast within the periodic cell. The same behavior also applies to the center frequency position of the band-gap in the dispersion diagram, which shifts to higher frequencies for higher w.

2.2. SIW with periodically etched CSRRs

The second configuration of periodic SIW has been obtained by periodically etching CSRRs on the waveguide surface. Fig. 3 shows the unit cell of period D of this second configuration of periodic SIW. Given that the CSRRs are resonant below the waveguide cutoff frequency [19,20], in order to obtain an equivalent center frequency of the pass-band to that in a periodically perforated SIW, a narrower waveguide with $a_{siw} = 12.4$ mm and lower period $D = 7.55$ mm has been chosen for the design, yielding a cutoff frequency of the initial SIW at about 4 GHz. After reviewing the possible configurations of CSRRs, a pair of identical CSRRs are

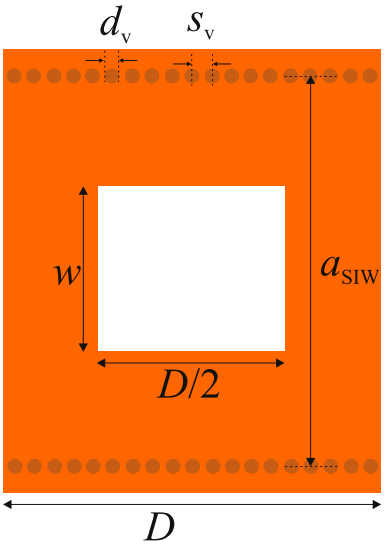

Fig. 1. Unit cell of a SIW with $a_{siw} = D = 23$ mm with periodic rectangular perforations of the substrate of dimensions $D/2 \times w$.

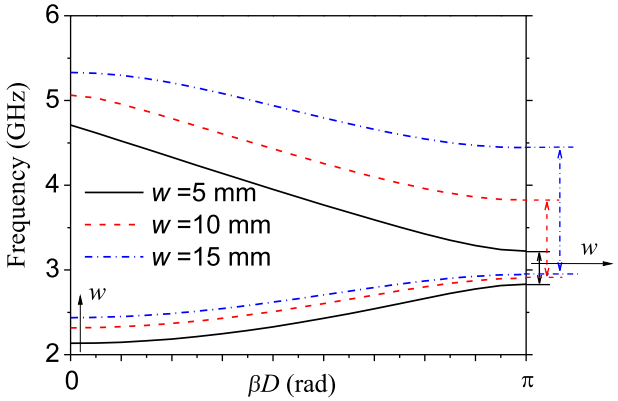

Fig. 2. Dispersion diagram of the periodically perforated SIW whose unit cell is shown in Fig. 1, for different values of the rectangle width w.

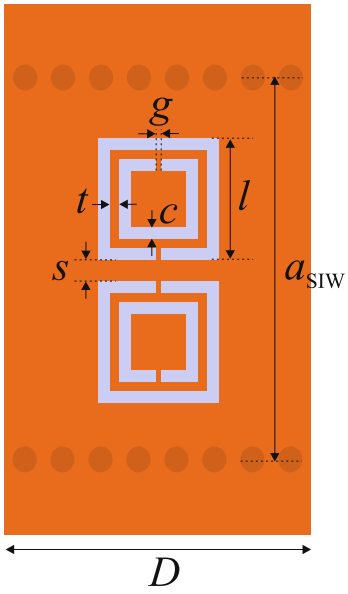

Fig. 3. Unit cell of a SIW with $a_{siw} = 12.4$ mm and $D = 7.55$ mm with periodically etched CSRRs. Geometrical parameters of the CSRRs: $l = 3.92$ mm, $c = 0.32$ mm, $s = 0.54$ mm, $t = 0.26$ mm, and $g = 0.18$ mm.

adopted and etched on the metal cover of the waveguide, in which the direction of the split of the outer rings are aligned face-to-face. The initial value of the geometrical parameters of the CSRRs in the unit cell, following [19], have been chosen as $l = 3.92$ mm, $c = 0.32$ mm, $s = 0.54$ mm, $t = 0.26$ mm and $g = 0.18$ mm. As in the previous subsection, a systematic study of the dispersion diagram as a function of the CSRRs geometrical parameters has been performed, when scaling the CSRRs to different factors f. Fig. 4 shows the dispersion diagram of the unit cell of Fig. 3 for three values of the scale factor f. As it can be appreciated, a small change in the CSRRs' size has a big effect in the dispersion diagram of the unit cell. First of all, the lower frequency pass-band of the waveguide shifts significantly to lower frequencies with the scale factor f. The same behavior is observed regarding the first band-gap position of the periodic structure, which shifts to lower frequencies as well, although its bandwidth remains nearly constant with f.

3. Filter designs and experimental verification

Although periodic structures have the property to generate pass-bands and stop-bands, they are not very suitable for filter

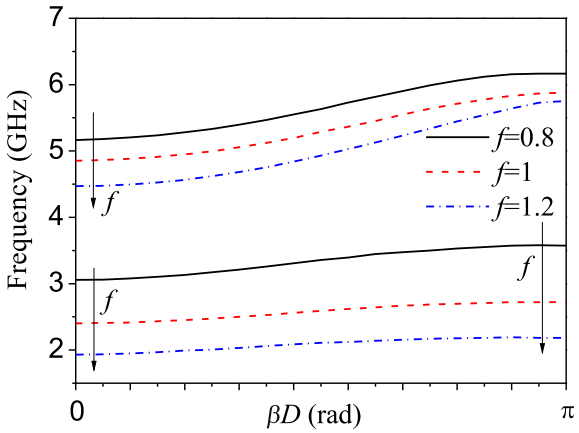

Fig. 4. Dispersion diagram of the SIW with periodically etched CSRRs whose unit cell is shown in Fig. 3 for different sizes of the CSRRs scaled by a factor f with respect to the values given in Fig. 3.

applications owing to lack of control on the bandwidth, return loss, etc. However, this section briefly discuss successful filter design procedures using the two proposed periodic SIWs, and following them, two band-pass filters based on the proposed periodic SIWs have been designed and fabricated. At this point, it is worth mentioning that, although a pair comparison of the obtained filters cannot be properly conducted due to the fact that both filters have different bandwidths (and also a different number of unit cells), this study will allow to extract the advantages and disadvantages of each filter configuration. In both filters, taper transitions from microstrip to SIW have been designed [7] and optimized. All simulations have been performed with Ansys HFSS.

The first filter consists of a periodically perforated SIW with 5 unit cells, whose scheme is shown in Fig. 5. The design of the filter parameters for obtaining a desired frequency response (center frequency, bandwidth and rejection band) has been directly carried out from the information provided in Fig. 2, and only a final optimization process of the parameters of the taper transitions has been done. The final parameters are: $a_{siw} = D = 23$ mm, $w = 10$ mm, $w_t = 1.58$ mm, $l_t = 10.8$ mm, $w_m = 0.6$ mm, $l_g = 11.5$ cm, $l_T = 14.7$ cm. The rectangular perforations have been covered with copper tape on both sides to avoid radiation losses. The simulated electrical response of the filter is represented in Fig. 7 in solid lines, along with the dispersion diagram of the first floquet mode of the structure in the pass-band (red line). A pass-band can be observed from 2.34 to 2.88 GHz, and a deep rejection band which extends up to 3.88 GHz (despite only 5 periods have been used). The return losses are higher than 12.5 dB in the pass-band, and insertion losses are lower than 2 dB from 2.45 GHz to 2.84 GHz (in the simulations, both dielectric ($\tan\delta = 0.0035$) and conductor ($\sigma_{Cu} = 5.8 \cdot 10^7$ S · m^{-1}) losses have been considered).

In Fig. 6 (top image) it is shown a photograph of the fabricated filter before covering the perforations with copper foil, adding the SMA connectors and soldering the copper vias. The prototype has been experimentally characterized: measurements have been performed in the frequency band from 1 to 5 GHz by using an Anritsu MS46122A vector network analyzer. No deembedding has been applied to the measured results, to remove the connectors and transitions effect. The comparison between simulations and measurements is shown in Fig. 7, and a good agreement is observed. The measured insertion loss is 1.66 dB at the central frequency $f_0 = 2.60$ GHz, compared to 1.52 dB in the simulation. Regarding the selective performance, the selectivity of the filter (expressed in dB/MHz, calculated from −10 dB in the measured response) is 0.284 dB/MHz in the lower transition band, and 0.131 dB/MHz in the upper transition band.

The simulation allows to investigate the different contribution of losses. Each transition contributes with a loss of 0.22 dB, whereas the SIW filter loss is 1.08 dB, attributed to the dielectric loss (0.7 dB) and to the conductor loss (0.38 dB). There is practically no radiation loss in the filter (0 dB). The size of the circuit is $l_g \times a_{SIW} = 2645$ mm^2.

A second periodic band-pass filter with the alternative configuration with CSRRs has been designed around the same frequency band, in this case with only 3 unit cells, i.e., 3 pairs of CSRRs etched on the SIW, given the significantly deeper rejection band that has been achieved, associated to the evanescent behavior of the waveguide. The scheme of this filter is shown in Fig. 8, and a photograph is provided in Fig. 6 (bottom image). Again, at the sight of the dispersion diagram of the unit cell (see Fig. 4), the center frequency, bandwidth and rejection band of the filter can be easily selected. A final optimization process of the parameters of the filter has been done, in which the size of the outer unit cells (CSRR1 in Fig. 8) has been slightly reduced with respect to the central one (indicated as CSRR2), as done in [18–20]. In order to obtain a similar center frequency than in the previous filter, the final parameters are: $a_{siw} = 12.4$ mm, $w_t = 1.9$ mm, $l_t = 8$ mm, $w_m = 0.6$ mm, $l_g = 2.1$ cm, $l_T = 5.3$ cm, $l_{ext} = 0.6$ mm, $l_R = 7.94$ mm; CSRR 1 parameters: same as in Fig. 3 caption; CSRR 2 has been scaled with respect to CSRR1 by a factor of 1.05. The simulated electrical response of the filter is represented in Fig. 9 with solid lines, along with the dispersion diagram of the first floquet mode of the structure in the pass-band (represented in red line). A narrower pass-band can be observed in this case from 2.47 to 2.7 GHz, and a deep rejection band which extends up to 5.06 GHz (with only 3 periods in this case). The return losses are higher than 19 dB in the pass-band, and insertion losses are lower than 2.0 dB from 2.53 GHz to 2.63 GHz. In order to check that there are no radiation losses in the resonators, the filter response has also been obtained

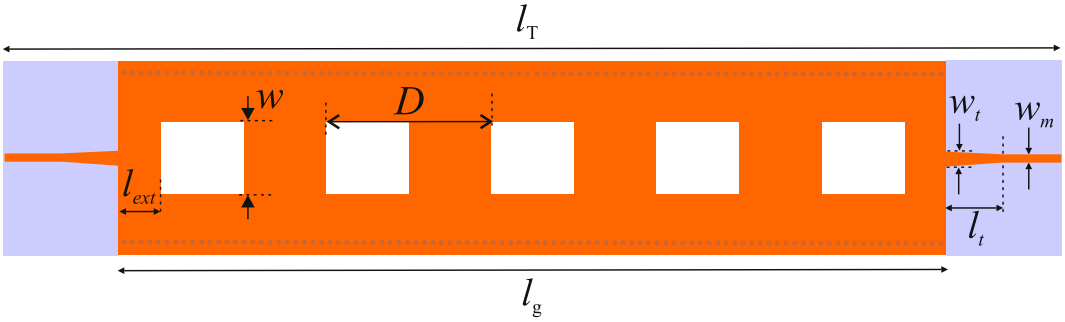

Fig. 5. Scheme of the periodically perforated SIW filter with 5 unit cells.

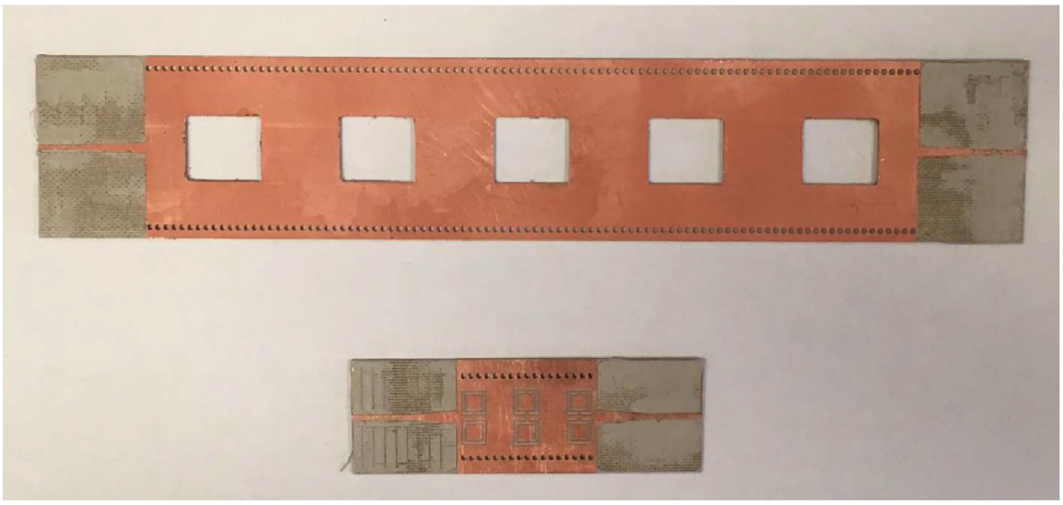

Fig. 6. Photograph of the fabricated periodic SIW filters.

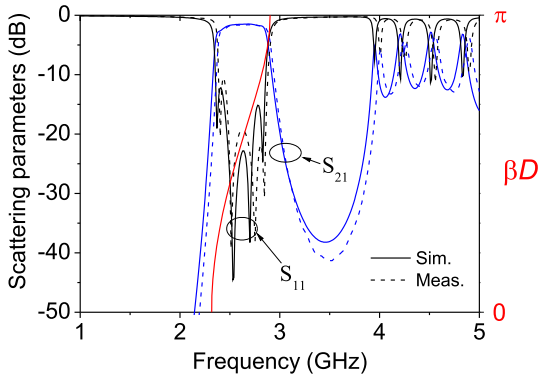

Fig. 7. Electrical response of the periodically perforated SIW filter (left axis) and dispersion diagram of the first floquet mode of the structure in the pass-band (red line, right axis). (For interpretation of the references to color in this figure legend, the reader is referred to the web version of this article.)

without material losses (see the dotted lines in the figure inset in Fig. 9), showing that the insertion losses are very low in the pass-band (lower than 0.2 dB), or, equivalently, that the resonators are not radiating energy.

This filter has also been fabricated. Fig. 6 (bottom image) shows a photograph of the filter before adding the SMA connectors and soldering the copper vias. In Fig. 9, the measured response of the filter (represented with dashed lines) is compared

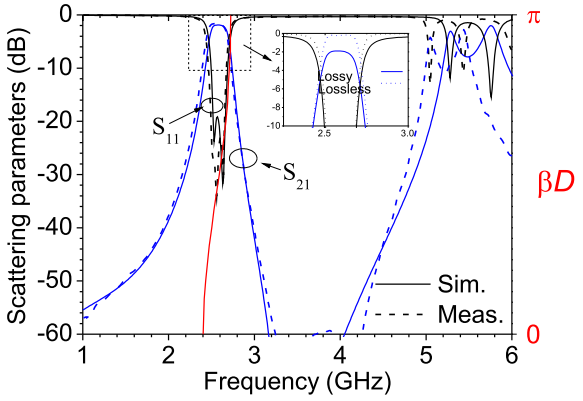

Fig. 9. Electrical response of the SIW filter with CSRRs (left axis) and dispersion diagram of the first floquet mode of the structure in the pass-band (red line, right axis). (For interpretation of the references to color in this figure legend, the reader is referred to the web version of this article.)

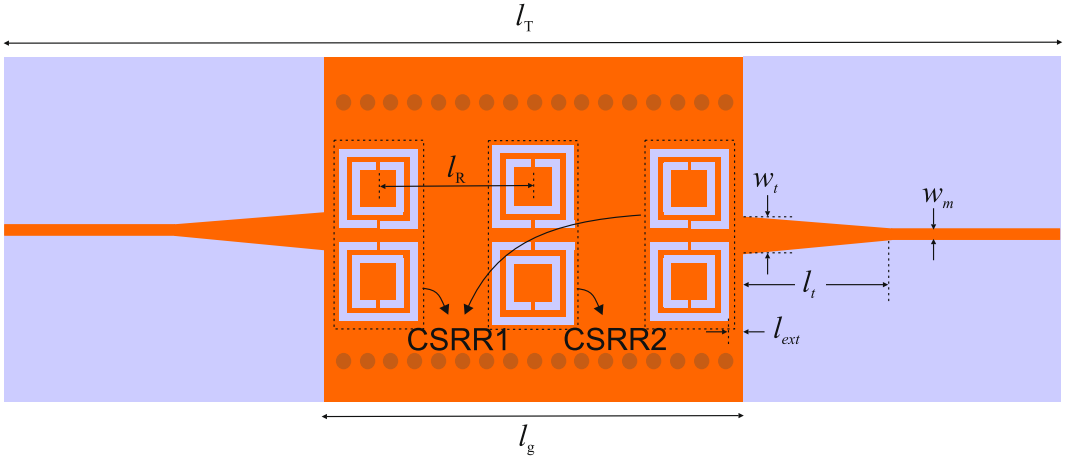

Fig. 8. Scheme of the SIW filter with CSRRs.

Table 1
Performance characteristics of the two fabricated periodic SIW filters.

	Center frequency (GHz)	Bandwidth (%)	Insertion Loss (dB)	Return Loss (dB)	Lower TBS* (dB/MHz)	Higher TBS* (dB/MHz)	Size (cm^2)
Filter 1	2.60	20	1.66	10.5	0.284	0.131	26.45
Filter 2	2.58	10	1.68	23	0.113	0.141	2.6

* TBS: Transition Band Selectivity.

with the simulated one (in solid line), and a good agreement is observed. The insertion loss at the central frequency $f_0 = 2.58$ GHz is 1.89 dB in the simulation and 1.68 dB in the measurement. Regarding the selective performance, in this case, the selectivity of the filter is 0.113 dB/MHz in the lower transition band, and 0.141 dB/MHz in the upper transition band. Also in this design, the different contribution of losses has been investigated through simulations. Each transition contributes with a loss of 0.18 dB, whereas the SIW filter loss is 1.53 dB, which is attributed to dielectric loss (0.9 dB), conductor loss (0.43 dB), and radiation loss (0.1 dB). The size of the circuit is significantly reduced compared with the case of the filter in Fig. 7, being the footprint area $l_g \times a_{SIW} = 260\ mm^2$.

Table 1 summarizes the performance characteristics of the two fabricated periodic SIW filter configurations (where Filter 1 stands for the periodically perforated filter, while Filter 2 is that with CSRR). Two main advantages can be observed in the CSRRs-based filter with respect to the perforated-based one. On the one hand, the total size is much smaller (with the total length being almost one third, and half the waveguide width), for a similar working frequency. On the other hand, its electrical response is much more selective, with a narrower pass-band, but also with a much wider and deeper rejection band, thus making this second topology more suitable for the design of selective filters in S-band. However, further investigations must be performed at higher frequency bands, in which a bigger electrical size may not be inconvenient from a resolution point of view in the manufacture of the circuits, and resonant structures may have higher losses.

4. Conclusion

Periodic SIWs have been applied to the analysis, design and comparison of two band-pass filters in S-band with different types of periodic cell, in order to highlight their advantages and disadvantages. A first filter consisting of periodic rectangular perforations of the dielectric substrate of the SIW has been compared with a second periodic SIW filter with square CSRRs etched on the waveguide surface. The dispersion diagram of the unit cell of each periodic structure has been obtained, showing the dependence of the width and location of the first pass-band and stop-band on the different parameters of the periodic cell, which has allowed the design of a periodic filter based on each proposed topology, highlighting their differences in terms of size and frequency response. Finally, it has been concluded that in the CSRRs-based filter, a much smaller filter with a more selective electrical response is obtained, thus making this second topology more suitable for the design of selective filters in S-band.

Acknowledgement

This work was supported by the Agencia Estatal de Investigación (AEI) and by the Unión Europea through the Fondo Europeo de Desarrollo Regional - Una manera de hacer Europa (AEI/FEDER, UE), under the research project TEC2016-75934-C4-2-R.

References

[1] Marini S, Soto P, Coves A, Gimeno B, Boria VE. Practical design of filters using EBG waveguides periodically loaded with metal ridges. Progr Electrom Res C 2016;63:13–21.
[2] Solano MA, Gómez A, Lakhtakia A, Vegas A. Rigorous analysis of guided wave propagation of dielectric electromagnetic band-gaps in a rectangular waveguide. Int J Electron 2005;92(2):117–30.
[3] Wang CC, Chiu HC, Ma TG. A slow-wave multilayer synthesized coplanar waveguide and its applications to rat-race coupler and dual-mode filter. IEEE Trans Microw Theory Tech 2011;59(7):1719–29.
[4] Chang WS, Chang CY. Novel microstrip periodic structure and its application to microwave filter design. IEEE Microw Wireless Comp Lett 2011;21(3):124–6.
[5] Gao MJ, Wu LS, Mao JF. Compact notched ultra-wideband bandpass filter with improved out-of-band performance using quasi electromagnetic bandgap structure. Progr Electrom Res 2012;125:137–50.
[6] Kurra L, Abegaonkar MP, Basu A, Koul SK. Switchable and tunable notch in ultrawideband filter using electromagnetic bandgap structure. IEEE Microw Wireless Comp Lett 2014;24(12):839–41.
[7] Deslandes D, Wu K. Integrated microstrip and rectangular waveguide in planar form. IEEE Microw Wireless Comp Lett 2001;11(2):68–70.
[8] Cassivi Y, Perregrini L, Arcioni P, Bressan M, Wu K, Conciauro G. Dispersion characteristics of substrate integrated rectangular waveguide. IEEE Microw Wirel Compon Lett 2002;12(9):333–5.
[9] Chen XP, Wu K. Substrate integrated waveguide filter: basic design rules and fundamental structure features. IEEE Microwave Mag 2014;15(5):108–16.
[10] Chen XP, Wu K. Substrate integrated waveguide filters: design techniques and structure innovations. IEEE Microwave Mag 2014;15(6):121–33.
[11] Chen XP, Wu K. Substrate integrated waveguide filters: practical aspects and design considerations. IEEE Microwave Mag 2014;15(7):75–83.
[12] Simsek S, Rezaeieh SA. A design method for substrate integrated waveguide electromagnetic bandgap (SIW-EBG) filters. AEU Int J Electron Commun 2013;67:981–3.
[13] Moitra S, Bhowmik PS. Modelling and analysis of Substrate Integrated Waveguide (SIW) and half-mode SIW (HMSIW) band-pass filter using reactive longitudinal periodic structures. AEU Int J Electron Commun 2016;70:1593–600.
[14] Aghayari H, Nourinia J, Ghobadi C, Mohammadi B. Realization of dielectric loaded waveguide filter with substrate integrated waveguide technique based on incorporation of two substrates with different relative permittivity. AEU Int J Electron Commun 2018;86:17–24.
[15] Coves A, Torregrosa-Penalva G, San-Blas AA, Sánchez-Soriano MA, Martellosio A, Bronchalo E, et al. A novel band-pass filter based on a periodically drilled SIW structure. Radio Sci 2016;51(7):328–36.
[16] Silvestri L, Massoni E, Tomassoni C, Coves A, Bozzi M, Perregrini L. A new class of SIW filters based on periodically perforated dielectric substrate. In: Proc. 46th Eur. Microw. Conf. (EuMC); Oct. 2016. p. 775–8.
[17] Silvestri L, Massoni E, Tomassoni C, Coves A, Bozzi M, Perregrini L. Substrate integrated waveguide filters based on a dielectric layer with periodic perforations. IEEE Trans Microw Theory Tech 2017;65(8):2687–97.
[18] López D, Coves A, Bronchalo E, Torregrosa G, Bozzi M. Practical design of a band-pass filter using EBG SIW technology. In: Proc. 48th Eur. Microw. Conf. (EuMC); Sep. 2018. p. 77–80.
[19] Dong YD, Yang T, Itoh T. Substrate integrated waveguide loaded by complementary split-ring resonators and its applications to miniaturized waveguide filters. IEEE Trans Microw Theory Tech 2009;57(9):2211–22.
[20] Martín F. Artificial transmission lines for RF and microwave applications. Wiley; 2015.
[21] Baena JD, Bonache JF, Martín F, Sillero RM, Falcone F, Lopetegi T, et al. Equivalent-circuit models for split-ring resonators and complementary split-ring resonators coupled to planar transmission lines. IEEE Trans Microw Theory Tech 2009;57(9):2211–22.
[22] Bonache J, Gil I, García-García J, Martín F, Marqués R, Sorolla M. Band pass filters for ultra wideband systems. 2005 IEEE antennas and propagation society international symposium, vol. 2A. p. 639–42.
[23] Coves A, Marini S, Gimeno B, Boria V. Full-wave analysis of periodic dielectric frequency-selective surfaces under plane wave excitation. IEEE Trans Antennas Propag 2012;60(6):2760–9.
[24] Coves A, Torregrosa-Penalva G, Vicent G, Bronchalo E, San Blas AA, Bozzi M. Modeling of perforated SIW structures and their application to the design of step-impedance microwave filters. In: Proc. IEEE MTT-S int. conf. numer. electromagn. multiphys. modeling optim. (NEMO2017); May 2017. p. 293–5.
[25] Joannopoulos JD, Meade RD, Winn JN. Photonic crystals. Princeton University Press; 1995.